FLAME AND EMISSION CHARACTERISTICS FROM NH_3/CH_4 COMBUSTION UNDER ULTRASONIC EXCITATION

by

Yi SU, Yifeng CHEN, Chunjie SUI, Tianjiao BI, Wei CHEN, and Bin ZHANG *

College of Electromechanical Engineering,
Qingdao University of Science and Technology, Qingdao, China

Original scientific paper
https://doi.org/10.2298/TSCI221008029S

As a high energy density hydrogen-rich carrier, ammonia (NH_3) is a highly promising carbon-free fuel. The large-scale industrial application of NH_3 is limited by its low reactivity and high NO_x emission. In this work, the flame and emission characteristics of ammonia/methane (NH_3/CH_4) non-premixed combustion were investigated under ultrasonic excitation. An experimental system was designed and built, including non-premixed combustion system, loading ultrasonic system, deflectionmography temperature measurement system and flue gas measurement system. Combustion and measurement experiments at different ultrasonic frequencies and NH_3/CH_4 blending ratios were carried out. Flame images and flue gas species concentrations under ultrasonic excitation were acquired. The 3-D temperature field was reconstructed. The influence of ultrasonic excitation at different frequencies on flame characteristics, flame temperature field and emission characteristics of the combustion process was analysed. The mechanism of NH_3/CH_4 combustion enhancement and emission reduction was revealed when the flame was ex-cited by ultrasonic waves. Results showed that part of the hydrocarbon fuels was replaced by NH_3 to reduce CO_2 emission. The height and color of the NH_3/CH_4 flame were changed and the high temperature area of the flame gradually expanded as ultrasonic acted on the flame. As ultrasonic frequency increased, the emission concentrations of unburned CH_4, unburned NH_3, and NO decreased significantly. The flame was ex-cited by ultrasonic waves, which reduced its local equivalent ratio, improved combustion efficiency and suppressed NO_x generation.

Key words*: NH_3 combustion, ultrasonic wave, emission characteristics, temperature distribution*

Introduction

One of the most interesting research hotspots in recent years has been the development of clean alternative energy to achieve the low carbonisation of energy production and industrial combustion. As a hydrogen-rich carrier with high energy density, NH_3 is referred to as *another kind of* H_2 [1]. The widespread use of NH_3 fuel is expected to accelerate the transition from *carbon-based* to *hydrogen-based* energy. The NH_3 has the benefits of zero carbon emission, mature manufacturing process and low cost storage and transportation, so NH_3 has great potential for use in energy and power systems [2]. However, it also has disadvantages, such as narrow flammability limit, low laminar flame propagation velocity, long ignition delay time, low flame temperature and high NO_x emission. The large-scale industrial application of

* Corresponding author, e-mail: zb-sh@163.com

NH_3 is hampered by its drawbacks. Therefore, the study of the combustion characteristics [3-5], reaction mechanisms [6-8] and application methods [9, 10] of NH_3 has become an appealing research frontier in the field of clean combustion in recent years.

Current methods for achieving the stable combustion of NH_3 mainly include mixed combustion with hydrocarbon fuels [11], optimisation of heat and mass transfer processes [12], increase of turbulence intensity [13], and external auxiliary technology [14]. In addition, problems of high NO_x emission whilst improving the reactivity of NH_3 must be urgently solved. The methods of high pressure and rich fuel are commonly used to investigate the emission control and generation mechanisms of NH_3 combustion pollutants. Based on a reduced mechanism, Okafor *et al*. [7] carried out the kinetic analysis of NH_3/CH_4/air combustion under high pressure conditions and found that increasing the pressure can suppress NO_x formation by reducing the pool of OH and O radicals. Existing experimental studies on the low NO_x combustion of NH_3 fuel are mostly applied in gas turbine combustion chambers with complex combustion conditions. Apply it to industrial burners is challenging. Valera-Medina *et al*. [15] explored NH_3/H_2 swirling combustion under rich flame conditions and showed that NO emission concentrations decreased monotonically with increasing equivalence ratios, ϕ, when ϕ was greater than 1.1. Rich NH_3 combustion strategies were adopted to achieve the goal of NO_x emission reduction. However, it tended to cause a large amount of unburned NH_3 to escape, at the same time, fuel consumption was increased.

In the quest to reduce pollutant emissions, researchers have found that the addition of acoustic waves to the combustion flow field has a significant effect on combustion and emission characteristics. Therefore, a large number of studies on the effects of acoustic fields on flames have been conducted. Research on forced acoustic waves to flames focuses on the combustion of fuels such as H_2, CH_4, and acetylene with a low/medium frequency acoustic field (f = 30-1000 Hz). Kim *et al.* [16] studied the relationship between the resonance frequency of a non-premixed jet H_2 flame and the concentration of NO_x emission. Acoustic excitation reduced NO_x concentration over a wide frequency range. Specifically, at the flame resonance frequency, NO_x concentration was significantly reduced. Guo *et al.* [17] experimentally investigated the influence of standing waves with different waveforms on the soot suppression effect from acetylene diffusion flame and discovered that the soot suppression efficiency increased linearly as acoustic energy increased. The results elucidated that the vortex generated by acoustic excitation can promote air entrainment, strengthen the mixing of upstream fuel and air and reduce the exposure time of the reactants in the high temperature region. The premixing effect created by acoustic excitation at the flame root causes the flame lift-off. The height of flame decreases and the reaction zone is widened. Thus, NO_x emission is reduced.

Ultrasonic wave frequency is higher than 20 kHz. In comparison audible sound waves, the ultrasonic waves have many characteristics, such as short wavelength, high energy, significant thermal relaxation absorption of gas molecules, good directivity, strong reflection ability and intensive acoustic energy, which can promote various physical and chemical effects. Scientists have made beneficial attempts to explore the combustion efficiency of the ultrasonic effect on the flames. Hirota *et al.* [18] experimentally explored the effect of CH_4/air laminar lifted flame ex-cited by ultrasonic waves. The results revealed that the improvement of the stability limit and the reduction of soot can be compatible in an appropriate range. Lee *et al.* [19] employed the schlieren method to discuss the influence of ultrasonic frequency on the behaviour of propane/air premixed flame. The study expounded that the flame propagation velocity increased as ultrasonic frequency increased. When ultrasonic excitation is applied to non-premixed NH_3/CH_4 combustion, its effect on flame and emission characteristics is expected.

In this study, an experimental system for the non-premixed NH_3/CH_4 combustion ex-cited by ultrasonic waves was constructed. The flame response characteristics of NH_3/CH_4 combustion were investigated under working conditions of different ultrasonic frequencies and different NH_3 blending ratios. The NH_3/CH_4 flame shapes were captured and discussed. Combustion temperature evolution laws were expounded on the basis of reconstructed NH_3/CH_4 combustion temperature fields. The emission rules of the main combustion process under different ultrasonic conditions were analysed. The emission reduction mechanisms of NH_3/CH_4 combustion ex-cited by ultrasonic waves were also revealed.

Experimental method and system

The deflectionmography was applied to measure the temperature distribution of combustion under ultrasonic excitation. Infrared photometry was employed to diagnose the species concentration of the combustion process ex-cited by ultrasonic waves. The experimental system included a combustion system, a loading ultrasonic system and a hybrid measurement system.

Combustion system

The burner is shown in fig. 1. The burner is mainly composed of the nozzle, fuel tube, air tube, uniform air-flow chamber and levelling bolts. A nozzle with frustum structure is installed on the top of the fuel tube. A hole diameter is 1.5 mm in the top of the nozzle. The inner and outer diameters of the fuel tube are 6.0 mm and 8.0 mm, respectively. Air-flows out of the uniform air-flow chamber and then into the annular channel between the air tube and fuel tube.

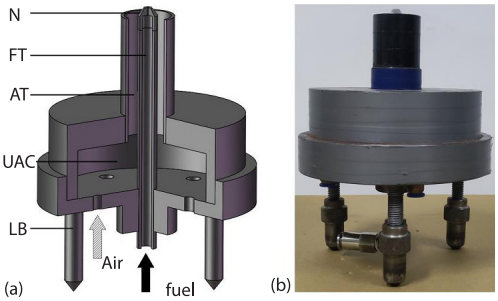

Figure 1. Structure of burner: *N – nozzle, FT – fuel tube, AT – air tube, UAC – uniform air-flow chamber, and LB – levelling bolts*

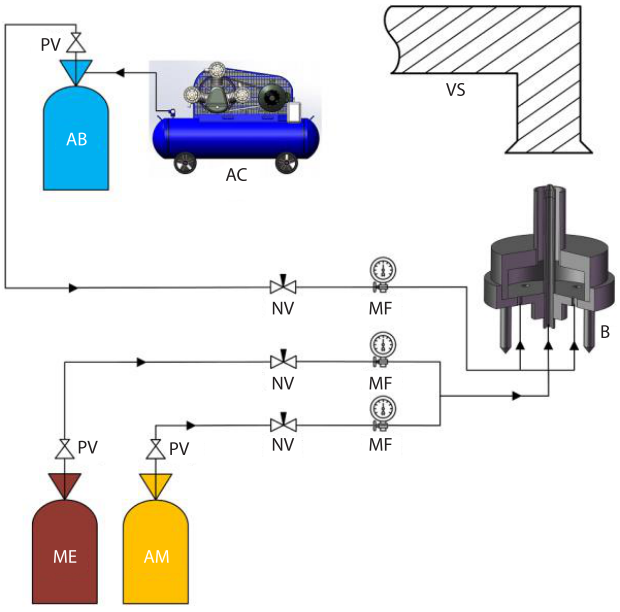

Figure 2. Combustion system: *AB – air bottle, AC – air compressor, AM – ammonia bottle, B – burner, ME – methane bottle, MF – mass-flow controller, NV – needle valve, PV – pressure-reducing valve, and VS – ventilation system*

The piping system is shown in fig. 2. The fuel piping includes NH_3 and CH_4 pipelines. The fuel flows out of the fuel bottles and into the fuel line through the pressure-reducing valves (reduced to 0.2 MPa), needle valves and mass-flow controllers (accuracy ±1%) in turn. The two branches, NH_3 and CH_4, are combined and ejected from the nozzle. The air is depressurised to 0.4 MPa by a pressure-reducing valve and passes through a needle valve and a mass-flow controller (accuracy ±1%) into the air line.

Ultrasonic device

The ultrasonic system comprises a signal generator, a power amplifier and an ultrasonic transducer. The signal generator emits electrical signals, which are amplified by a single-channel power amplifier. The ultrasonic transducers of different frequencies are driven by amplified signals. Electrical energy is converted into high frequency acoustic energy by an ultrasonic transducer. The location of the ultrasonic transducer is adjusted by a gripper. Three piezoelectric transducers of 20 kHz, 25 kHz, and 28 kHz are employed in this work. The maximum output frequency of the signal generator (RIGOL DG811) is 10 MHz, and the sampling rate is 125 MSa/s. The frequency resolution is 1 Hz, and the vertical resolution of the signal is 16 bits. The maximum output current of the power amplifier (ATA-68020, bandwidth 10-70 kHz) is 2.12 Ap. The output voltage gain is 0-300 times, and the maximum output power is 901 Wp.

Measurement method and system

A digital camera (Nikon D5600, 6000 dpi × 4000 dpi) is used to record the flame shape. The hybrid measurement system, fig. 3, is composed of an acoustic pressure measurement system, a deflectionmography temperature measurement system and a flue gas component measurement system.

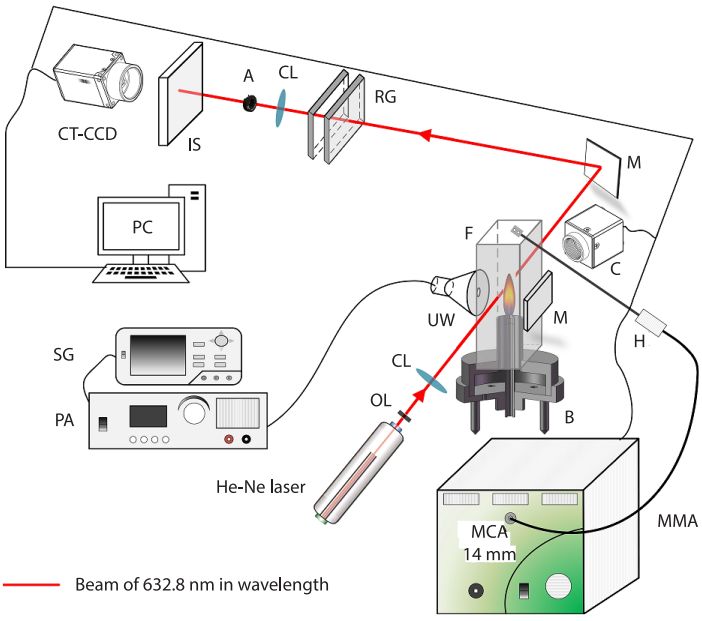

Figure 3. Hybrid measurement system: *A – aperture, B – burner, C – camera, CT-CCD, CT-CCD camera, F, – flue gas-collecting hood, H – heated measuring gas pipe, He-Ne laser, He-Ne laser, IS – image screen, CL – convex lens, M – mirror, MMA, mobile multicomponent analyser, OL – objective lens, PA – power amplifier, PC – personal computer, RG – Ronchi grating, SG – signal generator, and UW – ultrasonic transducer*

Deflectionmography temperature measurement

Deflectionmography is based on the principle that the direction of light is changed when light propagates in a non-uniform refractive index field. Thus, the data of integral projection are obtained. The reconstruction algorithm is then used to invert the 2-D refractive index distribution within the cross-sections. Parameter distributions, such as density and temperature, can also be obtained [20-22]. The precision of the refractive index measurement is 10^{-5}.

The beam emitted from the 10 mW He-Ne laser (λ = 632.8 nm) is expanded by the objective lens (25 × magnification), which is then collimated by the convex lens (diameter of 100.0 mm, focal length of 500.0 mm) into a parallel beam with a diameter of 55.0 mm. After passing through the region be measured, the parallel beam passes vertically through the Ronchi gratings (178 mm × 178 mm) placed in parallel. The spacing between the two Ronchi gratings is 30.0 mm, and the pitch of the Ronchi grating is 0.05 mm. The convex lens with a focal length of 500.0 mm is passed through the parallel beam. The beam is filtered by a small aperture to remove stray light. Finally, a CT-CCD camera (1024 dpi × 768 dpi, the maximum frame rate of 204) is used to capture the Moire fringe on the imaging screen.

Infrared measurements of gas components

The principle of the gas component measurement is based on the substance-specific extinction of infrared light. It is directed through the measuring gas where the lessening of the light intensity within the substance-specific absorption wave length is a degree for its concentration. The flue gas measurement system is composed of a mobile multicomponent analyser (MCA14m) and a flue gas-collecting hood with a size of 10.0 cm × 10.0 cm × 30.0 cm. The mobile multicomponent analyser can measure 11 flue gas components, including NO, NH_3, CO_2, and CH_4, *etc.* The measurement accuracy of the mobile multicomponent analyser is ±1% FS, and the resolution is 0.01 mg/m^3. The flue gas-collecting hood has square holes on both sides for placing the ultrasonic transducer and the reflector, as illustrated in fig. 3. During the measurement preparation, the temperature of the heated measuring gas pipe is preheated to 186 °C is to reduce measurement errors caused by heat loss from combustion products in the measuring gas pipe. The gas sample probe is positioned 10 cm above the flame. Data are updated every 20 seconds.

Experimental procedure and results

Combustion experiment with ultrasonic excitation

The hybrid measurement system was built, as presented in fig. 3. The air compressor was switched on, so the air was stored in the air bottle. The air with a flow rate of 0.1 m/s was supplied to create a stable combustion environment. The total fuel mass-flow rate was set to 180 standard cubic centimetres per minute (sccm). Valves of NH_3/CH_4 bottle and air bottle were switched on. When the NH_3/CH_4 was ejected from the nozzle, a torch was used to ignite blending fuel. The ultrasonic devices were then turned on, and the signal amplifier was set to 150 times. Then, the combustion flow field was acted on by ultrasonic waves. When the flame was stabilised, the CT-CCD camera and a digital camera were employed to, respectively capture the Moire fringes and flame images of NH_3/CH_4 combustion. The flue gas sampling analysis was started at the same time.

Three different frequencies of ultrasonic transducers and four different ratios of NH_3/CH_4 fuel were applied for the experiments. The experimental working conditions are shown in tab. 1.

Table 1. Experimental working conditions

No.	The CH_4 volume flow [sccm]	The NH_3 volume flow [sccm]	Frequency [kHz]
A	180	0	0/20/25/28
B	162	18	0/20/25/28
C	144	36	0/20/25/28
D	126	54	0/20/25/28

The NH_3/CH_4 flame characteristics with ultrasonic excitation

Figure 4 show flame images for the experimental working conditions corresponding to tab. 1. The X_{NH3} was defined as the mole fraction of NH_3 in blending fuel.

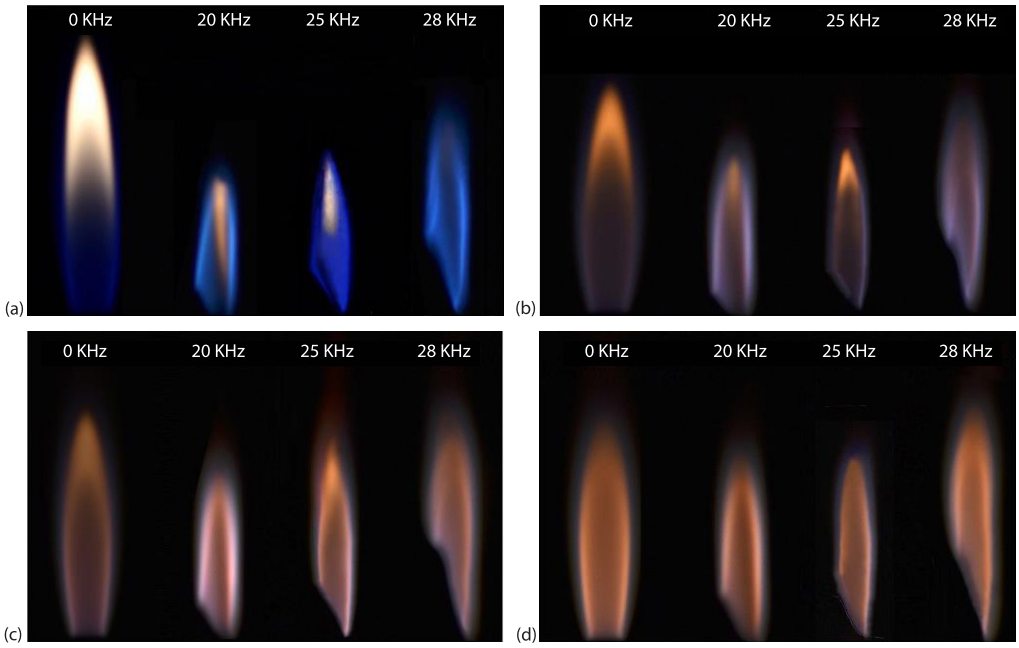

Figure 4. The NH_3/CH_4 flame ex-cited by ultrasonic waves of; (a) working Condition A, (b) working Condition B, (c) working Condition C, and (d) working Condition D

From working Condition A to working Condition D, fig. 4, when the flame was ex-cited by ultrasonic waves of different frequencies, a similar changing rule in the characteristics of the flame occurred as the fuel ratio changed. The flame height first became short and then increased as the ultrasonic wave frequency increased, when the flames were ex-cited by ultrasonic waves. When the forcing frequency increased, the flame curvature decreased and the flame height increased [23]. As the ultrasonic frequency increased, the trend for the inclination degree of upstream flame was similar. In fig. 5(a), the flame was stably burned when the burning velocity, S, at the flame front was the same as the velocity, V, of the local unburned gas-flow. When the flow field was affected by ultrasonic excitation, the flame and unburned gas-flow were inclined at an angle of α and θ, respectively, fig. 5(b). Local unburned gas-flow velocity, V, was perpendicular to the flamelet, which can be expressed as $V = V'\cos(\alpha + \theta) = S$. Assuming that

the flame burning velocity was constant, the $V' = S/\cos(\alpha + \theta)$ could be obtained. The velocity along the y-axis can be denoted as $V_{local} = V'\cos\theta = S\cos\theta/\cos(\alpha + \theta)$, which was greater than V. The angle of inclination of the flame was variable with the velocity of the unburned gas-flow, which meant that the addition of ultrasonic excitation increased the velocity of the unburned gas-flow. The α increased as ultrasonic frequency increased.

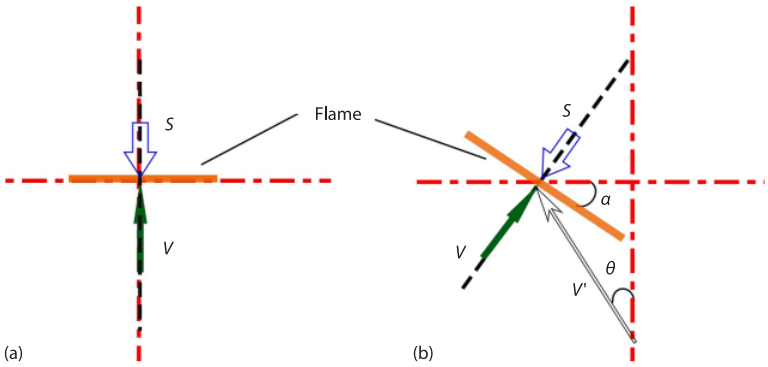

Figure 5. Stream line and flame inclined images; (a) without ultrasonic excitation and (b) with ultrasonic excitation

In fig. 4(a), the downstream of the flame without ultrasonic excitation appeared bright yellow, which was caused by the presence of soot in the downstream part of the flame. The flame structure was significantly affected by the pressure fluctuations around the flame caused by the ultrasonic waves. The mixing rate of air and flame increased, and the local ϕ of the flame reduced as ultrasonic frequency increased. Thus, the diffusion flame was changed to a flame with premixed characteristics. The flame ex-cited by ultrasonic waves was burned fully. The color of the flame gradually changed to blue because the amount of soot production was reduced.

The flame height decreased, and the flame color changed obviously as the proportion of NH_3 in the fuel increased. The addition of NH_3 reduced the reactivity of the blending fuel, resulting in low burning velocity in the flow field. The blue color of the flame was gradually replaced by orange yellow after the addition of NH_3 because the chemiluminescence of CH radical and CO_2 was blue [24] when CH_4 was burned, and NH_2-α radicals were orange yellow [25] when NH_3 was burned. The orange yellow appeared first in the downstream region of the flame, when small amounts of NH_3 were added to the CH_4 fuel. As the proportion of NH_3 increased, the flame gradually developed into orange yellow. In the meantime, the blue associated with the hydrocarbon flame was gradually weakened.

The NH_3/CH_4 combustion temperature distributions with ultrasonic excitation

The deflection information of light was extracted using the wave-front retrieval method. Figure 6 shows the reference Moire fringes and deflected Moire fringes of flame ex-cited by 25 kHz ultrasonic waves with $X_{NH_3} = 0.3$. Firstly, the Fourier frequency spectrum was obtained by a 2-D Fourier transform of the Moire fringes. Filter function was employed to extract the +1 order frequency spectrum. Then, inverse Fourier transform and phase unwrapping were performed to obtain the true phase of the deformed wavefront. The deflection angle data were further calculated through phase data. Subsequently, the reconstruction algorithm was employed to invert the refractive index distribution of the measured flow field using the deflection angle

data. Thereafter, the temperature distribution was calculated from the refractive index distribution via the Glastone-Dale formula. The 2-D temperature distributions of 20 cross-sections were reconstructed from the Moire fringes of each working condition. Then, the 2-D temperature distributions data of 20 cross-sections were coupled into a matrix of 3-D temperature values. Finally, the Visualization Toolkit was used to visualise the 3-D temperature distribution. The direct measurement method was applied to verify the validity of the deflectionmography temperature measurement. Under the same working conditions, a thermocouple was employed to measure the temperature field through multipoint and repeated measurements. The relative error of the temperature measurements between deflectionmography and direct measurement was 6.83%.

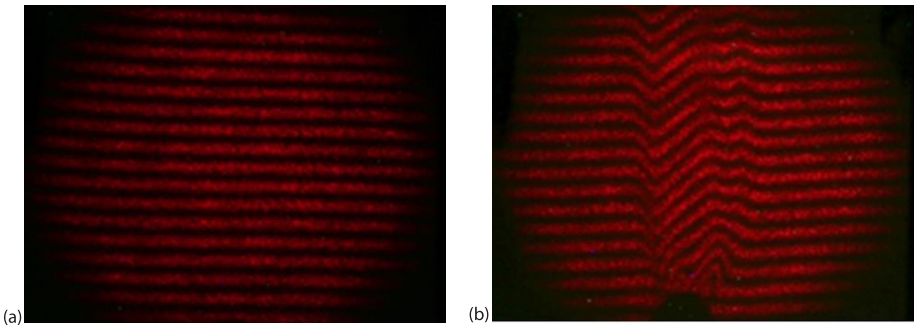

Figure 6. Moire fringes; (a) reference Moire fringes and (b) deflected Moire fringes

Flame images and longitudinal sections of flame temperature distributions were displayed simultaneously, as illustrated in figs. 7-10. Based on the reconstructed results, the flame temperature tended to increase and then decrease along the jet direction. A low temperature region appeared in the centre of the flame. The flame temperature first increased and then decreased from the centre to the edge of the flame, along the radial direction. Considering that the fuel sprayed out at the nozzle and spread around, the oxidant simultaneously diffused to the flame surface and entered the gas side to react where air and fuel were mixed significantly and molecules were collided violently. Therefore, this area had the highest temperature. When the fuel was ejected a certain distance out of the nozzle, the reaction was gradually weakened and the heat was lost in the downstream of the flame. Therefore, the flame temperature gradually decreased in the axial direction.

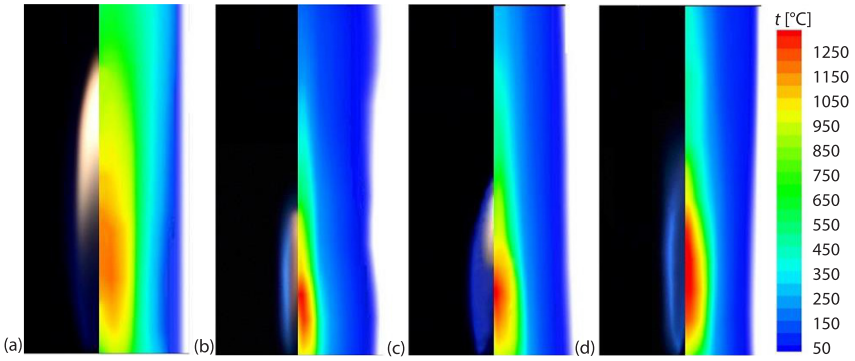

Figure 7. Temperature distribution of CH_4 flame ex-cited by ultrasonic waves of; (a) 0 kHz, (b) 20 kHz, (c) 25 kHz, and (d) 28 kHz

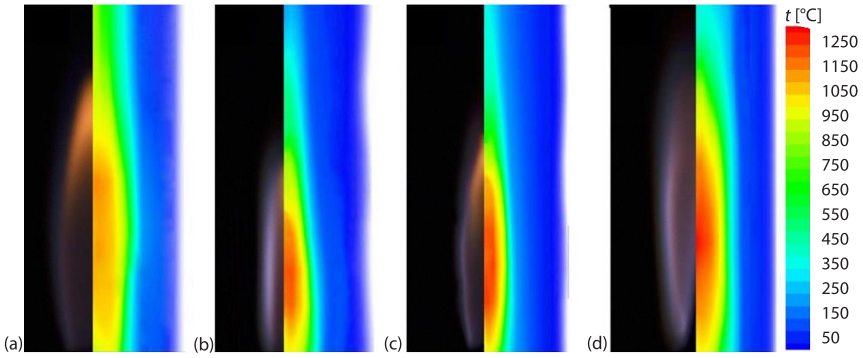

Figure 8. Temperature distribution of flame ex-cited by ultrasonic waves of; (a) 0 kHz, (b) 20 kHz, (c) 25 kHz, and (d) 28 kHz with X_{NH_3} = 0.1

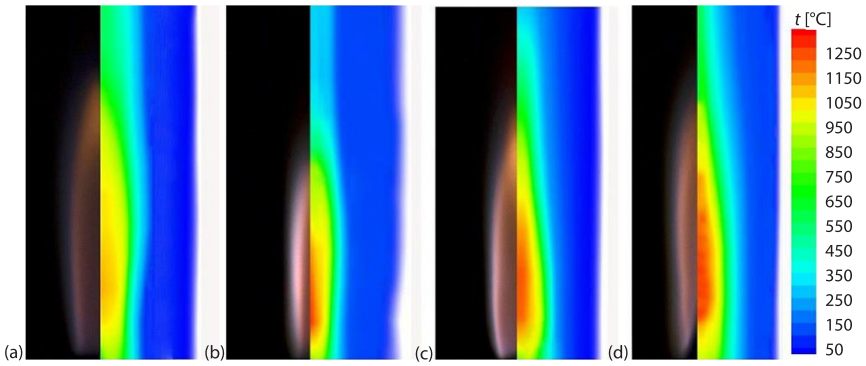

Figure 9. Temperature distribution of flame ex-cited by ultrasonic waves of; (a) 0 kHz, (b) 20 kHz, (c) 25 kHz, and (d) 28 kHz with X_{NH_3} = 0.2

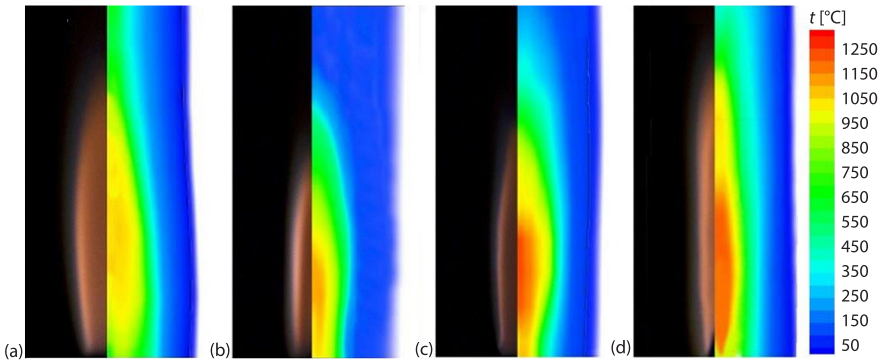

Figure 10. Temperature distribution of flame ex-cited by ultrasonic waves of; (a) 0 kHz, (b) 20 kHz, (c) 25 kHz, and (d) 28 kHz with X_{NH_3} = 0.3

The combustion working conditions ex-cited by 28 kHz ultrasonic waves were taken as an example to analyse the evolution law of the flame temperature field at different X_{NH3}. From figs. 7-10, the maximum flame temperature decreased as X_{NH_3} increased. The maximum flame temperature of pure CH_4, X_{NH_3} = 0.1, X_{NH_3} = 0.2, and X_{NH_3} = 0.3 were 1310 °C, 1263 °C, 1204 °C, and 1178 °C, respectively. Compared with the pure CH_4 flame, the maximum tem-

perature of different X_{NH3} flame dropped by 3.59%, 8.09%, and 10.08% as X_{NH_3} increased. At the same ultrasonic frequency, the high temperature region of the flame gradually reduced as X_{NH_3} increased. Owing to the low calorific value of NH_3, the flame temperature decreased as X_{NH_3} increased. In addition, due to the low reactivity of NH_3, a large amount of activation energy was required to maintain combustion. The NH_3 absorbed part of the heat released by the combustion of CH_4, which resulted in a low maximum temperature in the flow field due to the addition of NH_3 to the fuel.

The experimental conditions of flame with $X_{NH_3} = 0.1$ were used as examples to analyse the law of flame temperature distributions as the ultrasonic frequency changed. As the ultrasonic frequency increased from 0 kHz to 20 kHz, 25 kHz, and 28 kHz, the maximum temperature of flame gradually increased. The area of the high temperature region increased as ultrasonic wave frequency increased. The maximum temperatures were 1079 °C, 1160 °C, 1203 °C, and 1263 °C in the $X_{NH_3} = 0.1$ flame applied with 0 kHz, 20 kHz, 25 kHz, and 28 kHz ultrasonic waves, respectively. Compared with the free flame without acoustic field, the maximum flame temperature of $X_{NH_3} = 0.1$ increased by 7.51%, 11.50%, and 17.05% as ultrasonic frequency increased. Compared with the flame temperature without ultrasonic excitation, the amplification of maximum flame temperature for pure CH_4, $X_{NH_3} = 0.2$ and $X_{NH_3} = 0.3$, respectively, increased by 14.61%, 17.62%, and 16.74% when flames were ex-cited by 28 kHz ultrasonic waves. Pressure fluctuation occurred around the flame when it was ex-cited by ultrasonic waves. Reactants were diffused efficiently in the ultrasonic wave fields, which enhanced the mixing of fuel and air. The diffusion flame became a flame with premixed characteristics. The flame temperature and the reaction rate of the combustion process increased under the continuous ultrasonic excitation.

Emission characteristics of NH_3/CH_4 combustion with ultrasonic excitation

The measurement of flue gas component concentration was performed. When the combustion was stable, multiple measurements were carried out and the values of multiple measurements were averaged.

Figure 11 show the emission characteristics of unburned CH_4 and CO_2 with ultrasonic frequency for blending fuel (pure CH_4, $X_{NH_3} = 0.1$, $X_{NH3} = 0.2$, and $X_{NH_3} = 0.3$). When the ultrasonic frequency that ex-cited the flame was the same, the concentration of unburned CH_4 and CO_2 of flue gas decreased accordingly as X_{NH_3} increased. When the 20 kHz ultrasonic wave was applied to the flame, the CO_2 and unburned CH_4 emission concentration of the flame with $X_{NH_3} = 0.3$ decreased by 32.01% and 27.90%, respectively, compared with the pure CH_4 flame. The addition of NH_3 reduced the mole fraction of CH_4 in the blending fuel correspondingly. The generated CO_2 also decreased, which achieved the expectation of reducing CO_2 emission. For the same fuel blending ratio, CO_2 emission concentration increased as ultrasonic frequency increased. At the same X_{NH_3}, the unburned CH_4 concentration of combustion emission had been declining as ultrasonic frequency increased. When the flame with $X_{NH_3} = 0.1$ was ex-cited by ultrasonic waves, the CH_4 emission concentration decreased by 14.91%, 29.04%, and 41.67% with ultrasonic frequencies from 20 kHz, 25-28 kHz, respectively, compared with no external action. When 28 kHz ultrasonic ex-cited a flame with pure CH_4, $X_{NH_3} = 0.2$ and $X_{NH3} = 0.3$, the CH_4 emission concentration decreased by 40.65%, 44.19%, and 51.62%, respectively, compared with the flame without ultrasonic excitation. Compared with the flame without ultrasonic, the maximum increase of CO_2 reached 100.01% in working Condition D. That is, the carbon conversion was complete during the combustion process.

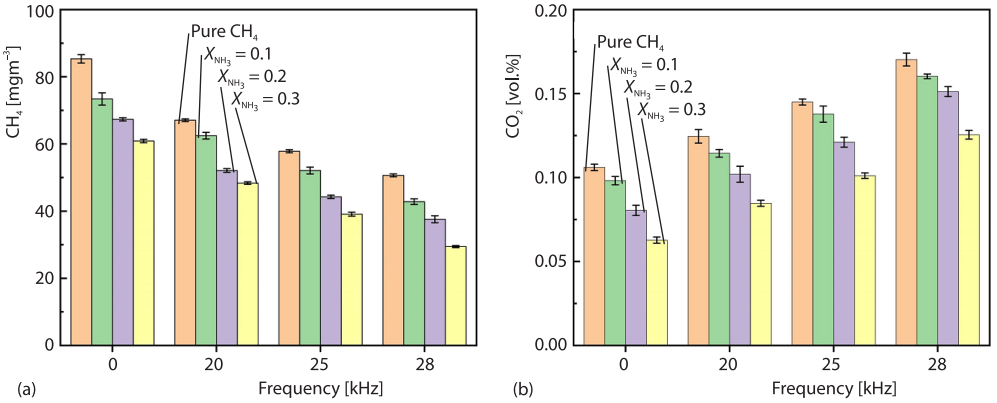

Figure 11. Unburned CH_4 and CO_2 concentration variation with frequency at different fuel ratios

The emission characteristics of NO and unburned NH_3 for different working conditions are displayed in fig. 12, respectively. When the ultrasonic frequency that ex-cited the flame was the same, NO and unburned NH_3 increased as X_{NH_3} increased. At the same X_{NH_3}, the emission concentrations of NO and unburned NH_3 decreased as ultrasonic frequency increased. The largest reduction in NO concentration was 46.45% for flame with $X_{NH_3} = 0.1$ ex-cited by 28 kHz ultrasonic waves. When the flame with $X_{NH_3} = 0.3$ was ex-cited by 28 kHz ultrasonic waves, the unburned NH_3 concentration decreased the most, which was 54.86%.

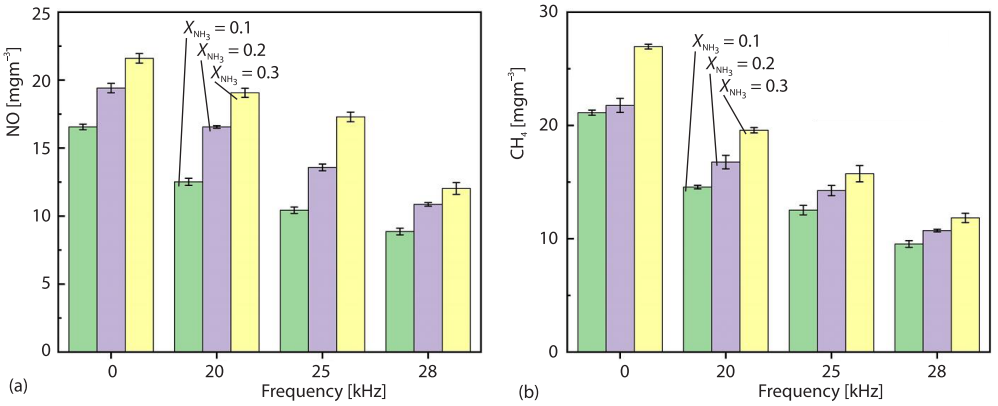

Figure 12. The NO and unburned NH_3 concentration variation with frequency at different fuel ratios

From the aforementioned phenomenon, the flame structure was changed by the ultrasonic wave field, the flame height was reduced and the flame was lifted. The fuel contacted and reacted with sufficient air, which meant that many O radicals entered the reaction area. The diffusion rate of the fuel and the mixing rate of the fuel and air were increased, contributing to the widening of the violent reaction area. The addition of high frequency acoustic waves increased the collision probability amongst the species in the reaction area. The blending homogeneity of the species was improved and the local equivalence ratio of flame was reduced. The further oxidation of carbonaceous compounds, such as CO in combustion, was promoted, which allowed additional unburned CH_4 to participate in the reaction. The heat and mass transfer processes were enhanced during the reaction process, and the combustion efficiency was improved. As illustrated in fig. 11, the CO_2 emission concentration increased and the unburned CH_4 emission

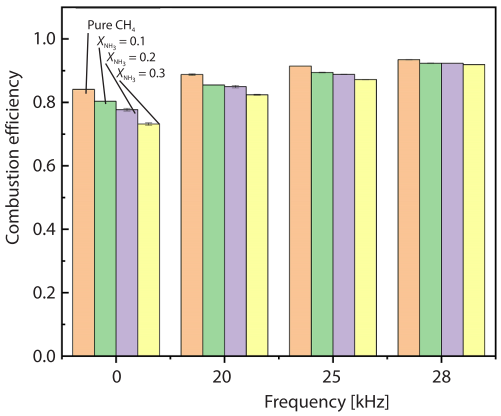

Figure 13. Combustion efficiency variation with frequency at different fuel ratios

concentration decreased as ultrasonic frequency increased. When the flame was ex-cited by ultrasonic waves, the flame exhibited premixed characteristics. At the same time, the ultrasonic effect promoted the sufficient contact between the intermediate combustion product NO and the unburned NH_3, which may trigger the selective non-catalytic reduction reaction. Figure 12 display that the emission concentrations of unburned NH_3 and NO decreased as ultrasonic frequency increased, that is, NH_3 was burned fully and pollutant emissions were effectively suppressed under ultrasonic excitation. Figure 13 showed the dependence of combustion efficiency on the ultrasonic wave frequency for different working conditions. At the same X_{NH_3}, the combustion efficiency increased as ultrasonic wave frequency increased.

Conclusion

The use of NH_3 offers a new idea for the development of the energy industry. However, the direct combustion of NH_3 as a fuel has shortcomings of poor combustion stability and high NO_x emission. In this study, the ultrasonic loading system and simultaneous multiparameter measurement system of combustion were constructed. The effects of ultrasonic excitation on combustion enhancement and pollutant reduction were explored when the NH_3/CH_4 non-premixed flames were ex-cited by ultrasonic waves. Based on the study of ultrasonic characteristics, ultrasonic waves of different frequencies were loaded in NH_3/CH_4 flames with different ratios. Flame shapes, flame colors, temperature distributions and component concentrations were obtained to analyse the law of NH_3/CH_4 combustion influenced by ultrasonic excitation. The results indicated that part of the hydrocarbon fuels was replaced by NH_3 to reduce CO_2 emission. As ultrasonic excitation was added to the combustion flow field, the flame height decreased, the flame color was changed, the high temperature region of the flame was expanded and the combustion temperature was increased. Furthermore, the combustion process of NH_3/CH_4 was enhanced. At the same time, the unburned NH_3 and NO_x in the flue gas emissions reduced significantly, and the combustion efficiency increased as ultrasonic frequency increased. Consequently, ultrasonic excitation, as a physical action, is expected to be used in the industrial combustion optimisation of NH_3 fuel.

Acknowledgment

This work was supported by the Natural Science Foundation of Shandong Province of China (No. ZR2021ME131).

Nomenclature

f – frequency, [Hz]
S – burning velocity [ms^{-1}]
V – unburned gas-flow velocity [ms^{-1}]
X_{NH_3} – mole fraction of species NH_3, [–]

Greek symbols

α – flame angle, [°]
θ – unburned gas-flow angle, [°]
λ – wavelength, [nm]
ϕ – equivalence ratio, [–]

References

[1] Kobayashi, H., *et al*., Science and Technology of Ammonia Combustion, *Proc. Combust. Inst.*, *37* (2019), 1, pp. 109-133
[2] Elbaz, A. M., *et al.*, Review on the Recent Advances on Ammonia Combustion From the Fundamentals to the Applications, *Fuel Commun*., *10* (2022), 100053
[3] Shu, T., *et al.*, An Experimental Study of Laminar Ammonia/Methane/Air Premixed Flames Using Expanding Spherical Flames, *Fuel*, *290* (2021), 120003
[4] Ji, L., *et al*., Experimental Study on Structure and Blow-off Characteristics of NH_3/CH_4 Co-Firing Flames in a Swirl Combustor, *Fuel*, *314* (2022), 123027
[5] Somarathne, K. D. K. A., *et al.*, Modelling of Ammonia/Air Non-Premixed Turbulent Swirling Flames in a Gas Turbine-Like Combustor at Various Pressures, *Combust. Theory Model.*, *22* (2018), 5, pp. 973-997
[6] Tian, Z., *et al*., An Experimental and Kinetic Modelling Study of Premixed $NH_3/CH_4/O_2$/Ar Flames at Low Pressure, *Combust. Flame*, *156* (2009), 7, pp. 1413-1426
[7] Okafor, E. C., *et al*., Measurement and Modelling of The Laminar Burning Velocity of Methane-Ammonia-Air Flames at High Pressures Using a Reduced Reaction Mechanism, *Combust. Flame*, *204* (2019), June, pp. 162-175
[8] Mathieu, O., Petersen, E. L., Experimental and Modelling Study on the High-Temperature Oxidation of Ammonia and Related NO_x Chemistry, *Combust. Flame*, *162* (2015), 3, pp. 554-570
[9] Juangsa, F. B., *et al*., The CO_2-Free Power Generation Employing Integrated Ammonia Decomposition and Hydrogen Combustion-Based Combined Cycle, *Therm. Sci. Eng. Prog*., *19* (2020), 100672
[10] Cardoso, J. S., *et al*., Ammonia as an Energy Vector: Current and Future Prospects for Low-Carbon Fuel Applications In Internal Combustion Engines, *Journal Clean. Prod*., *296* (2021), 126562
[11] Dai, L., *et al.*, Ignition Delay Times of NH_3/DME Blends at High Pressure and Low DME Fraction: RCM Experiments And Simulations, *Combust. Flame*, *227* (2021), May, pp. 120-134
[12] Chen, Y., *et al.*, Effect and Mechanism of Combustion Enhancement and Emission Reduction for Non-Premixed Pure Ammonia Combustion Based on Fuel Preheating, *Fuel*, *308* (2022), 122017
[13] Khateeb, A. A., *et al*., Stability Limits and Exhaust NO Performances of Ammonia-Methane-Air Swirl Flames, *Exp. Therm. Fluid Sci*., *114* (2020), 110058
[14] Ju, Y., Sun, W., Plasma Assisted Combustion: Dynamics and Chemistry, *Prog. Energy Combust. Sci*., *48* (2015), June, pp. 21-83
[15] Valera-Medina, A., *et al.*, Premixed Ammonia/Hydrogen Swirl Combustion under Rich Fuel Conditions For Gas Turbines Operation, *Int. J. Hydrogen Energy*, *44* (2019), 16, pp. 8615-8626
[16] Kim, M., *et al*., Flame-Vortex Interaction and Mixing Behaviors of Turbulent Non-Premixed Jet Flames under Acoustic Forcing, *Combust. Flame*, *156* (2009), 12, pp. 2252-2263
[17] Guo, H., *et al*., Influence of Acoustic Energy on Suppression of Soot from Acetylene Diffusion Flame, *Combust. Flame*, *230* (2021), 111455
[18] Hirota, M., *et al*., Soot Control of Laminar Jet-Diffusion Lifted Flame Ex-Cited by High-Frequency Acoustic Oscillation, *Journal Therm. Sci. Technol.*, *12* (2017), 2, pp. 1-10
[19] Lee, S. S., *et al*., An Experimental Study on the Structural Alteration of C3H8-Air Premixed Flame Affected by Ultrasonic Standing Waves of Various Frequencies, *Journal Mech. Sci. Technol*., *29* (2015), 3, pp. 917-922
[20] [20] Su, Y., *et al*., The 3-D Velocity and Temperature Distribution Measurement and Characteristic Analysi of Swirling Combustion, *Measurement*, *193* (2022), 110949
[21] Zhang, B., *et al*., Flame Four-Dimensional Deflectionmography with Compressed-Sensing-Revision Re-Construction, *Opt. Lasers Eng*., *83* (2016), Aug., pp. 23-31
[22] Zhang, B., *et al*., Deflectionmographic Reconstructions of a 3-D Flame Structure and Temperature Distribution Oo Premixed Combustion, *Appl. Opt*., *54* (2015), 6, 1341
[23] Ahn, M., *et al.*, Effects of Acoustic Excitation on Pinch-off Flame Structure and NO_x Emissions in H_2/CH_4 Flame, I*nt. J. Hydrogen Energy*, *47* (2022), 26, pp. 13178-13190
[24] Mikofski, M. A., *et al*., Flame Height Measurement of Laminar Inverse Diffusion Flames, *Combust. Flame*, *146* (2006), 1-2, pp. 63-72
[25] Hayakawa, A., *et al*., Laminar Burning Velocity And Markstein Length of Ammonia/Air Premixed Flames at Various Pressures, *Fuel*, *159* (2015), Nov., pp. 98-106

Paper submitted: October 8, 2022
Paper revised: January 4, 2023
Paper accepted: January 5, 2023